2014 14th IEEE-RAS International Conference on
Humanoid Robots (Humanoids)
November 18-20, 2014. Madrid, Spain

Virtual Model Control for Dynamic Lateral Balance

Ruta Desai, Hartmut Geyer and Jessica K. Hodgins

Abstract— **Motivated by an interest in human-like controllers for humanoids to increase their social acceptance, we investigate lateral balancing for artistic performances on challenging surfaces. Control design for lateral balancing in humanoids has primarily focused on optimal control techniques. While these techniques generate balancing controllers, it remains unclear whether humans use similar strategies. Here we propose that humans prefer intuitive task-space control for lateral balancing on simple as well as challenging surfaces. We develop a virtual model controller for this task and compare with simulations of a planar model, the resulting balancing behavior against human lateral balancing on flat ground and on a seesaw as an example of a challenging surface. We find that the proposed controller can be tuned to respond to balance disturbances on flat ground in a human-like way, and that it mimics human behavior on a seesaw including the failure to stabilize the board, even though an optimal LQR controller is capable of stabilizing it. The results support the hypothesis that humans prefer intuitive control in lateral balancing and suggest that state-of-the-art control approaches in robotics may go beyond what humans can accomplish. These limitations should be taken into account when designing human-like controllers for humanoids.**

I. Introduction and Related Work

Similar to [1] and [2], we are interested in human-like controllers for humanoids, because they may increase the social acceptance of robots performing in entertainment environments. Our current focus is on lateral balancing strategies, in particular for artistic performances on challenging surfaces like a seesaw or a bongo board.

Control of humanoid robots has primarily been designed for walking and sagittal plane balancing [3], [4]. Lateral balancing on challenging surfaces is less often addressed, although significant active control might be essential in this case [5]. For lateral balance of a humanoid on a seesaw, Anderson and Hodgins [6] proposed an inverse dynamics policy mixing controller that uses optimization to match desired contact forces and joint accelerations. They also later proposed a cascade framework with receding horizon control that robustly balanced a robot on a bongo board in simulation [7]. Hyon [8] distributed contact forces in a feedforward manner and then used a global center of mass (COM) controller to achieve balance. Recently, Nagarajan and Yamane [9] proposed a universal controller for lateral balance using output feedback. Using feedback of global pelvis position and velocity as well as the global foot angle, their controller robustly stabilized a robot model in lateral balancing on a variety of challenging surfaces including a seesaw, a bongo board, and curved and tilted surfaces. However, it remains unclear whether these different control strategies are similar to human control approaches for the same balancing tasks. For instance, while humans may be optimizing for metabolic cost and stability [14], they might not be able to find the optimal gains needed for the generalized controller of [9] or LQR, which requires optimizing future costs (value function) for infinite horizon. Nor might they be able to perform the finite but longer term planning required by the receding horizon control in [7].

Direct hypotheses about human control of lateral balancing are rare. Human control strategies in the sagittal and lateral planes are believed to be distinct, based on observed joint torques [10], [11]. Hence, hypotheses about sagittal plane control cannot be directly used to explain lateral balancing. Winter [10] investigated possible error signals and control policies for lateral balance during standing and walking in humans. He suggested that the difference between the center of pressure (COP) and center of mass (COM) positions is a probable error signal used for lateral stabilization in humans. The hypothesis was supported in mediolateral perturbation experiments of human standing by Rietdyk and Matjačić [11], [12]. While explicit control strategies like ankle, hip and stepping strategies are known for sagittal balancing, such control strategies for lateral balancing still need to be identified [10].

We propose that humans prefer an intuitive task-space control for lateral balancing on simple as well as challenging surfaces. Evidence of task space control in humans has been found in studies of goal directed arm or eye-saccadic movements, which showed that humans seem to minimize the variance in the end-point position of these redundant movements [13]. Further evidence for end-point control is found in the impedance control literature, where experiments suggest that humans control the magnitude, shape and orientation of endpoint stiffness [14]. We hypothesize that humans try to minimize the variance in the COM position and trunk orientation in lateral balancing tasks, and that designing a corresponding humanoid controller will produce human-like balancing behavior. Towards testing this hypothesis, we here develop a virtual model control of human or humanoid balancing and compare with simulations of a planar model the resulting balancing behavior against human lateral balancing on flat ground and on a seesaw. Virtual model control is a simplified, intuitive version of task space control that neglects segment dynamics. It has been introduced for walking by Pratt and colleagues [15] and successfully been used by Hoffmann and colleagues [16] to simulate human behavior during one-legged balancing.

In Sec. II, we present the planar model and develop the

The authors are with Carnegie Mellon University, Pittsburgh, 5000 Forbes Avenue, Pittsburgh, PA 15213, USA. {rutad, hgeyer, jkh}@cs.cmu.edu

virtual model controller for lateral balancing on flat ground and on a seesaw as an example of a challenging surface. We then show in Sec. III that the resulting model can be tuned to respond to disturbances in a human-like way. We further show that the proposed control as well as humans fail to balance on the seesaw, even though an optimal LQR controller is capable of balancing (Sec. IV).

II. Approach

A. Model on Flat Ground

The flat-ground model represents a human(oid) in two-legged standing posture (Fig. 1). The upper body is modeled as a single trunk link with mass M and inertia I_t. The trunk is rigidly connected to a pelvis link of length $2d_p$ with point masses $m_t << M$ at each end (open circles in Fig. 1). The leg segments are massless and connected by revolute hip joints describing the adduction and abduction degree of freedom of human hips. The human knee primarily moves in the sagittal plane, effectively changing the leg length when projected to the frontal plane ($L^{l/r}$). This effect of knee motion is captured in the model with telescopic joints. The feet are modeled as point masses $m_f << M$ that are attached at the end of each leg and connected to the ground with rotational degrees of freedom which describes the ankle joint.

The hip joints and the telescoping leg joints are actuated, generating hip torques $\tau_h^{l/r}$ (positive torque describes extension) and leg forces $F_l^{l/r}$ (which can only be positive, extension forces). We neglect ankle actuation as the human ankle moment arms are small in the frontal plane, and hip loading and unloading has been observed as the dominant policy in lateral balancing with hip moments contributing 85% of the total moments during perturbations [10],[12]. Further, balance experiments with lower-limb amputees confirmed that amputees had greater problem controlling dynamic balance in the anteroposterior direction than the mediolateral direction, suggesting that ankle might not be as important for balance in the lateral plane as in the sagittal plane [17].

B. Controller for Lateral Balance on Flat Ground

The model has three degrees of freedom (DOF). These can be described by the horizontal (x) and vertical position (y) of the trunk COM and by the rotation of the trunk (θ_t) about the Z axis perpendicular to the frontal plane. We formulate the lateral balancing problem as maintaining desired states for these three DOFs and use virtual model control [15] to design an intuitive controller (Fig. 1B).

If the model is in a perturbed pose, virtual forces f_x, f_y, and f_t are generated as

$$\begin{aligned} f_x &= k_{px}(x^d_{com} - x_{com}) - k_{dx}\dot{x}_{com} \\ f_y &= (M + 2m_t)g + k_{py}(y^d_{com} - y_{com}) - k_{dy}\dot{y}_{com} \\ f_t &= k_{pt}(\theta^d_t - \theta_t) - k_{dt}\dot{\theta}_t \end{aligned} \quad (1)$$

to restore the position of the trunk and its global orientation. Here, x^d_{com}, y^d_{com} and θ^d_t are the desired trunk COM positions and desired trunk orientation with respect to the global

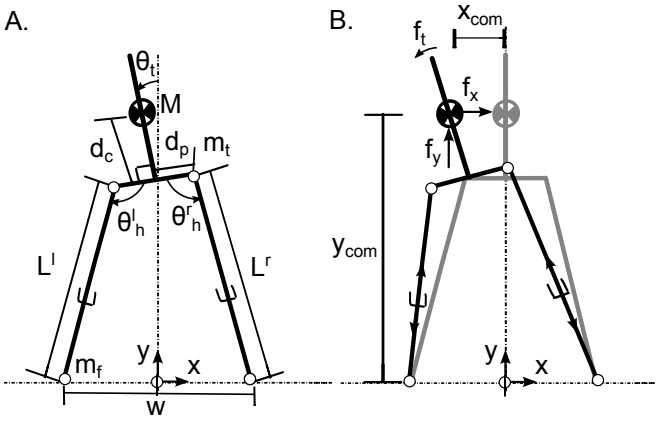

Fig. 1. Planar model on flat ground. (A) The configuration variables and mass properties of the model are shown. Arrows at the joints show positive angle and torque conventions. The task space coordinate system is shown by x-y located at the origin. The distance d_c is the height of trunk COM from the pelvis along the trunk, and w denotes the step width. (B) The model is shown in a perturbed pose with desired virtual forces and the target pose (in grey). The desired virtual forces f_x and f_y are applied to the trunk COM. The virtual force f_t denotes the torque desired to be applied at the trunk COM to control the global trunk angle θ_t.

vertical axis, the term $(M + 2m_t)g$ in the vertical force compensates gravity, and g is the gravitational acceleration. The gains $k_{px}, k_{dx}, k_{py}, k_{dy}, k_{pt}$ and k_{dt} are the proportional and derivative feedback gains of virtual PD controllers, which control the stiffness of COM in task space. The desired virtual forces are mapped into the model's joint torques under the static assumption $\boldsymbol{\tau} = J^T\mathbf{f}$, where $\mathbf{f} = [f_x\ f_y\ f_t]^T$ and J is the Jacobian relating trunk velocities to joint velocities.

1) Jacobian computation: The planar model forms a closed chain mechanism, and the COM of the trunk can be considered as its end-effector. We derive separate Jacobians for the left and right legs, J_L and J_R, respectively. For each leg, the configuration space vector $[\theta_h^{l/r}\ L^{l/r}\theta_t]^T$ includes the hip angle, the leg length, and the global trunk angle. The ankle angle is omitted, as it can be substituted using the hip and global trunk angles. The global trunk angle can be estimated in humans via the vestibular system. For humanoid applications, an IMU at the robot's trunk is required in addition to joint sensors to implement the proposed control. The trunk's COM x and y positions are

$$\begin{bmatrix} x^{l/r}_{com} \\ y^{l/r}_{com} \end{bmatrix} = \begin{bmatrix} \mp\frac{w}{2} \mp L^{l/r}c(\theta_h^{l/r} \mp \theta_t) - d_c s(\theta_t) \pm d_p c(\theta_t) \\ L^l s(\theta_h^{l/r} \mp \theta_t) + d_c c(\theta_t) \pm d_p s(\theta_t) \end{bmatrix}, \quad (2)$$

where l/r and $\pm$ indicate the path through the left or right leg, $c()$ and $s()$ represent cosine and sine functions, d_c and d_p are geometric link constants, and w is the distance between the feet (Fig. 1A). The resulting left and right legs' Jacobians, J_L and J_R, are given by .

$$J_{L/R} = \begin{bmatrix} \pm A & \mp cos(\theta_h^{l/r} \mp \theta_t) & -A \mp d_p sin(\theta_t) - d_c cos(\theta_t) \\ B & sin(\theta_h^{l/r} \mp \theta_t) & \mp B \pm d_p cos(\theta_t) - d_c sin(\theta_t) \\ 0 & 0 & 1 \end{bmatrix} \quad (3)$$

where $A{=}L^{l/r}s(\theta_h^{l/r}{\mp}\theta_t)$ and $B{=}L^{l/r}c(\theta_h^{l/r}{\mp}\theta_t)$.

2) Actuator torques: For each leg, the joint torques and leg force can be related to the virtual force generated at the trunk as

$$\begin{bmatrix}\tau_h^l\\ F_l^l\\ \tau_t^l\end{bmatrix} = J_L^T \begin{bmatrix}f_{xl}\\ f_{yl}\\ f_{tl}\end{bmatrix}, \begin{bmatrix}\tau_h^r\\ F_l^r\\ \tau_t^r\end{bmatrix} = J_R^T \begin{bmatrix}f_{xr}\\ f_{yr}\\ f_{tr}\end{bmatrix}, \tag{4}$$

where the total virtual force is given by the sum of the legs' virtual forces,

$$\begin{bmatrix}f_x\\ f_y\\ f_t\end{bmatrix} = \begin{bmatrix}f_{xl}\\ f_{yl}\\ f_{tl}\end{bmatrix} + \begin{bmatrix}f_{xr}\\ f_{yr}\\ f_{tr}\end{bmatrix}. \tag{5}$$

Eqs. 4 and 5 relate six joint torques to three desired virtual forces. However, the legs have no actuators between trunk segment and world frame, introducing the two constraints $\tau_t^{l/r} = 0$, which, substituted into Eq. 4, lead to

$$\begin{aligned} &f_t - f_{tr} + (f_y - f_{yr})(x_{com}^l + \frac{w}{2}) - (f_x - f_{xr})y_{com}^l = 0,\\ &f_{tr} + f_{yr}(x_{com}^r - \frac{w}{2}) - f_{xr}y_{com}^r = 0 \end{aligned} \tag{6}$$

where $(x_{com}^l, y_{com}^l) = (x_{com}^r, y_{com}^r)$. Furthermore, from Eq. 5, we obtain

$$\begin{aligned} f_{xl} &= f_x - f_{xr}\\ f_{yl} &= f_y - f_{yr}\\ f_{tl} &= f_t - f_{tr}. \end{aligned} \tag{7}$$

Substituting Eq. 7 into Eq. 6, reduces the two equations to the three unknowns f_{xr}, f_{yr} and f_{tr}. To solve for all the unknown variables, we introduce the additional constraint

$$f_{xr} = f_{xl} = \frac{f_x}{2} \tag{8}$$

on the virtual horizontal forces, leading to

$$\begin{aligned} f_{tr} &= f_{xr}(y_{com}) + f_{yr}(d_r - x_{com})\\ f_{yr} &= \frac{f_\theta + f_y(\frac{w}{2} + x_{com}) - f_x(y_{com})}{w} \end{aligned} \tag{9}$$

for the remaining unknowns. Finally, the actuator torques that generate the net desired virtual forces are obtained by applying Eq. 4.

C. Extension to Seesaw Balance

The seesaw is modeled as a rigid board of mass m_b and inertia I_b, which pivots about a revolute joint located at the board's center (Fig. 2). The human(oid) model on the seesaw is the same as in Sec. IIA. The only difference is that now the model's feet are contacting the seesaw board.

In addition to the three trunk DOFs (Sec. II B), the task space now includes the board angle θ_b making the net DOFs of the model to be four. We extend the virtual model control and introduce f_b as the force required to stabilize the board angle, given by a virtual PD control

$$f_b = k_{pb}(\theta_b^d - \theta_b) + k_{db}(0 - \dot{\theta}_b), \tag{10}$$

where $\theta_b^d = 0$ is the desired global board angle measured from the horizontal axis, and k_{pb} and k_{db} are the proportional and derivative gains.

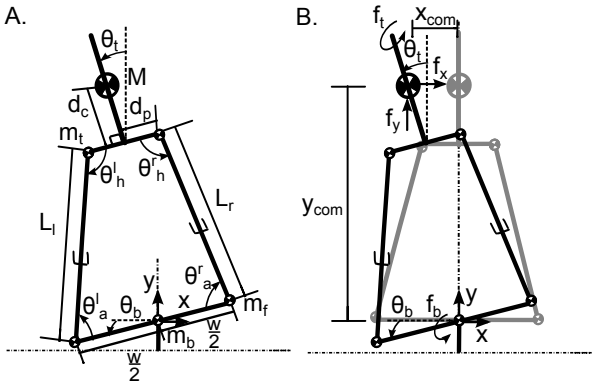

Fig. 2. Planar model on seesaw. (A) The configuration variables now include the global board angle θ_b. (B) The model is shown in a perturbed pose with desired pose shown in grey. f_b denotes the desired virtual force applied at the seesaw's pivot joint to control the global board angle. See caption of Fig. 1 for additional explanations.

1) Jacobian computation: The configuration space vector for each leg is now given by $[\theta_a^{l/r}\ L^{l/r}\ \theta_h^{l/r}\ \theta_t]^T$, where the ankle angle has been added to represent the global board angle (which cannot be measured directly in humans) with internal joint angles and the global trunk angle,

$$\theta_b^{l/r} = \mp\theta_a^{l/r} \mp \theta_h^{l/r} + \theta_t \pm \pi. \tag{11}$$

The trunk's COM x and y positions are given by .

$$\begin{bmatrix}x_{com}^{l/r}\\ y_{com}^{l/r}\end{bmatrix} = \begin{bmatrix}\pm\frac{w}{2}c(\theta_a^{l/r}{+}\theta_h^{l/r}{\mp}\theta_t){\mp}A{-}d_cs(\theta_t){\pm}d_pc(\theta_t)\\ -\frac{w}{2}s(\theta_a^{l/r}{+}\theta_h^{l/r}{\mp}\theta_t){+}B{+}d_cc(\theta_t){\pm}d_ps(\theta_t)\end{bmatrix} \tag{12}$$

with $A = L^{l/r}c(\theta_h^{l/r}{\mp}\theta_t)$ and $B = L^{l/r}s(\theta_h^{l/r}{\mp}\theta_t)$. The left and right Jacobians resolve to .

$$J_{L/R} = \begin{bmatrix}\mp\frac{w}{2}c(\sigma_1) & \mp c(\sigma_2) & \pm L^{l/r}s(\sigma_2) \mp \frac{w}{2}c(\sigma_1) & A\\ -\frac{w}{2}s(\sigma_1) & s(\sigma_2) & L^{l/r}c(\sigma_2) - \frac{w}{2}s(\sigma_1) & B\\ \mp 1 & 0 & \mp 1 & 1\\ 0 & 0 & 0 & 1\end{bmatrix}, \tag{13}$$

where $\sigma_1 = \theta_a^{l/r} + \theta_h^{l/r} \mp \theta_t$, $\sigma_2 = \theta_h^{l/r} \mp \theta_t$, $A = -d_cc(\theta_t) \mp d_ps(\theta_t) - L^{l/r}s(\sigma_2) + \frac{w}{2}s(\sigma_1)$ and $B = -d_cs(\theta_t) \pm d_pc(\theta_t) \mp L^{l/r}c(\sigma_2) + \frac{w}{2}c(\sigma_1)$.

2) Actuator torques: Like the virtual forces f_x, f_y and f_t, the desired virtual board force can be divided into left and right leg components,

$$f_b = f_{bl} + f_{br}. \tag{14}$$

The actuator torque vectors for the left and right leg can then be written as

$$\begin{bmatrix}\tau_a^l\\ F_l^l\\ \tau_h^l\\ \tau_t^l\end{bmatrix} = J_L^T \begin{bmatrix}f_{xl}\\ f_{yl}\\ f_{bl}\\ f_{tl}\end{bmatrix}, \begin{bmatrix}\tau_a^r\\ F_l^r\\ \tau_h^r\\ \tau_t^r\end{bmatrix} = J_R^T \begin{bmatrix}f_{xr}\\ f_{yr}\\ f_{br}\\ f_{tr}\end{bmatrix}. \tag{15}$$

As the ankle joints are passive and the trunk cannot be actuated with respect to the world frame, we obtain four constraint equations $\tau_a^{l/r} = 0$ and $\tau_h^{l/r} = 0$ with .

$$\begin{bmatrix} \tau_a^l \\ \tau_t^l \\ \tau_a^r \\ \tau_t^r \end{bmatrix} = \begin{bmatrix} -f_{bl} - \frac{w}{2} f_{yl} c(\theta_a^l + \theta_h^l - \theta_t) + \frac{w}{2} f_{xl} s(\theta_a^l + \theta_h^l - \theta_t) \\ f_{bl} + f_{tl} + f_{yl} x_{com}^l - f_{xl} y_{com}^l \\ f_{br} - \frac{w}{2} f_{yr} c(\theta_a^r + \theta_h^r + \theta_t) + \frac{w}{2} f_{xr} s(\theta_a^r + \theta_h^r + \theta_t) \\ f_{br} + f_{tr} + f_{yr} x_{com}^r - f_{xr} y_{com}^r \end{bmatrix}. \tag{16}$$

Rearranging $\tau_t^l = 0$ and $\tau_t^r = 0$ in Eq. 16, we obtain a linear relationship,

$$f_b + f_t + f_y x_{com} - f_x y_{com} = 0, \tag{17}$$

between the four desired virtual forces at any COM position. This relationship implies that we cannot choose all four virtual forces independently, even though the model has four actuators. Thus, we cannot achieve the desired state for all four DOFs in task space simultaneously.

We prioritize three goals to resolve this issue. The virtual force f_y holds the model against gravity and the virtual force f_t keeps the trunk upright. Both goals are important in general locomotion including balancing. Hence, we maintain f_y and f_t using Eq. 1. Between f_x and f_b, we choose to control f_x as in Eq. 1 and solve for f_b in terms of f_x, f_y and f_t using Eq. 17 instead of obtaining f_b in a proportional-derivative fashion as in Eq. 10. To obtain the actuator torques, we further assume the design constraint

$$f_{tr} = f_{tl} = \frac{f_t}{2} \tag{18}$$

and solve for f_{xr}, f_{yr} and f_{br} using the first three equations in Eq. 16. Subsequently, f_{xl}, f_{yl} and f_{bl} can be obtained using Eqs. 5 and 14.

III. Results

A. Comparison to Human Lateral Balance on Flat Ground

We first check if the proposed control can generate human-like balance recovery. For this purpose, we try to replicate a typical human balance recovery experiment during quiet standing based on the experimental results reported in [12]. The mass parameters of the model in Fig. 1 are set to approximately match the human subjects in the experiments (see Tab. I, segment masses and lengths are scaled using anthropomorphic data in [18]). The controller gains are manually tuned. Furthermore, we add zero mean and unit variance gaussian noise for joint measurements (range: [-0.01 0.01] radians) and current and desired trunk COM position estimations (range: [-5 5] cm) to account for the noise that is present in the human nervous system [19].

The model starts from the desired pose in Fig. 1B where a disturbance of peak impulse magnitude $22.8Ns$ is applied to the pelvis from the right side (Fig. 3). The COM is perturbed and the trunk sways in the direction of perturbation. The controller recovers the model from the disturbed pose and returns it back into the desired pose (Fig. 3). The smoothed trajectories of COM-COP displacement, trunk sway, and hip torques for the model's response are compared in Fig. 4 to those trajectories of a human subjected to a similar disturbance. While we used the trunk sway motion to guide our manual gain tuning for Fig. 4A ($k_{px}, k_{dx}, k_{py}, k_{dy}, k_{pt}$ and k_{dt} in Tab. I are tuned to match trunk sway of the model to human data), the control also produces COM-COP displacement trajectories that compare to humans in magnitude (Fig. 4B). However, the recovery torques at the hip in the model differ from those in humans especially at the ipsilateral side (Fig. 4C). Torque at the contralateral hip, dominantly responsible for the recovery, differs only in peak magnitude. The deviation in the hip torques could be caused by differences in inertial properties between humans and the model, in which the leg masses are concentrated at the hip.

TABLE I

Control gains and model parameters for flat ground disturbance simulation.

parameter	value	parameter	value
body weight (bw)	86 kg	d_c	0.3130 m
M	0.6780×bw kg	d_p	0.1750 m
m_t	0.1×bw kg	w	0.35 m
m_f	0.0610×bw kg	I_t	1.6 kgm^2
k_{px}, k_{py}	750 Nrad^{-1}	k_{pt}	60 Nrad^{-1}
k_{dx}, k_{dy}	220 Nsrad^{-1}	k_{dt}	25 Nrad^{-1}

Note that because we manually tuned the gains in Tab. I, a combination of gain values different than the ones mentioned in Tab. I might also produce trajectories similar to those in Fig. 4A.

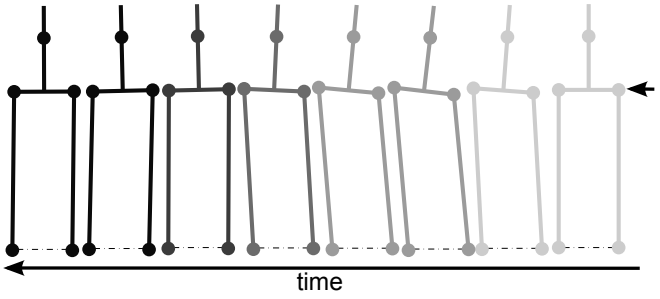

Fig. 3. Planar model on flat ground recovers from a disturbance of impulse amplitude 22.8Ns, applied at the right pelvis (indicated by arrow). Bold circles represent the location of segment masses in the model as in Fig. 1.

B. Seesaw Balance

The linear relationship between the virtual forces (Eq. 17) requires giving up one of the four goals in task space. We chose to give up the goal of maintaining board angle and solve for the virtual force f_b to obtain the controller as described in Sec. II-C. If we start from an initial disturbed pose, this controller brings the trunk's COM x and y positions to their desired values and uprights the trunk while constantly rocking the seesaw (Figs. 5B and 6). The rocking of the seesaw continues until the errors in these three goals converge to zero. After that the controller makes no effort to stabilize the board angle. The board remains in a configuration where one of its ends is in contact with the

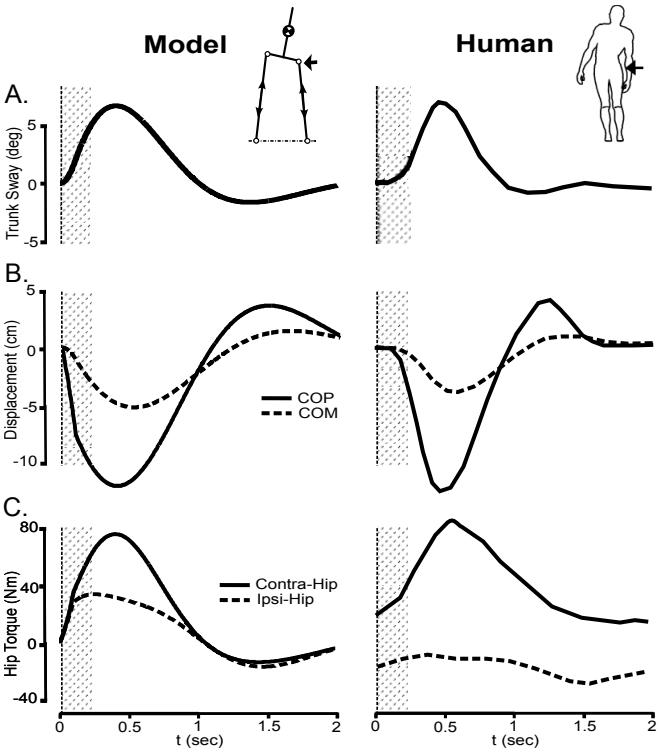

Fig. 4. Comparison of disturbance recovery response between proposed control and humans on flat ground. Trunk sway motion (A), COM-COP displacement (B), and hip torques are shown (C). The shaded patch indicates when the disturbance is active. Human responses are obtained from [12]. Controller gains are tuned to match trunk sway of the model to human data in (A), which also produces COM-COP displacement trajectories that compare to humans in magnitude in (B).

ground and the model remains in a configuration with upright trunk and COM in its desired position.

If humans use a similar control framework for lateral balancing, they should be subjected to the same constraint on task-space goals. To test if this could be the case and if giving up controlling the board angle goal might explain human behavior on a seesaw, we captured the motion of an expert at bongo board balancing on a seesaw (Fig. 5A). Although the subject explored various strategies like changing COM height, different feet alignment, rocking the board at high frequency and balancing with locked and unlocked knees, the subject could not stabilize the seesaw and the board repeatedly hit the ground on one end or the other. Similar behavior was observed for other subjects. The goal of achieving a desired board angle seems to be compromised in humans just as it is in the proposed control.

For a more qualitative comparison, we adapt the model's mass and inertia to the subject and start the simulation using initial conditions from the experimental data. We also add noise in joint measurements and trunk COM state estimation as described in Sec. IIIA. The noise prevents the controller from driving the error in COM position and trunk angle to zero, resulting in an intermittent rocking motion of the board in simulation, which visually looks very similar to a human balancing on a seesaw. Fig. 6 compares data

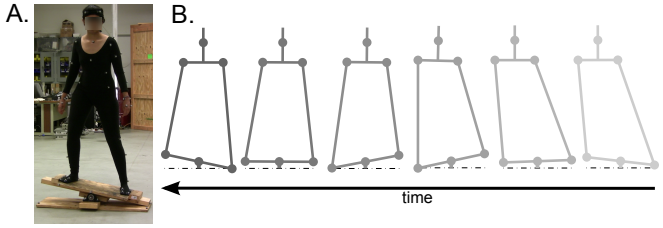

Fig. 5. Rocking motion of seesaw in humans and in simulation (A) A subject balancing on a seesaw during a motion capture study keeps rocking the board in an attempt to stabilize it but never succeeds in doing so. (B) The rocking motion in simulation is an outcome of virtual model control when giving up the task space goal of stabilizing the board angle and introducing sensor noise.

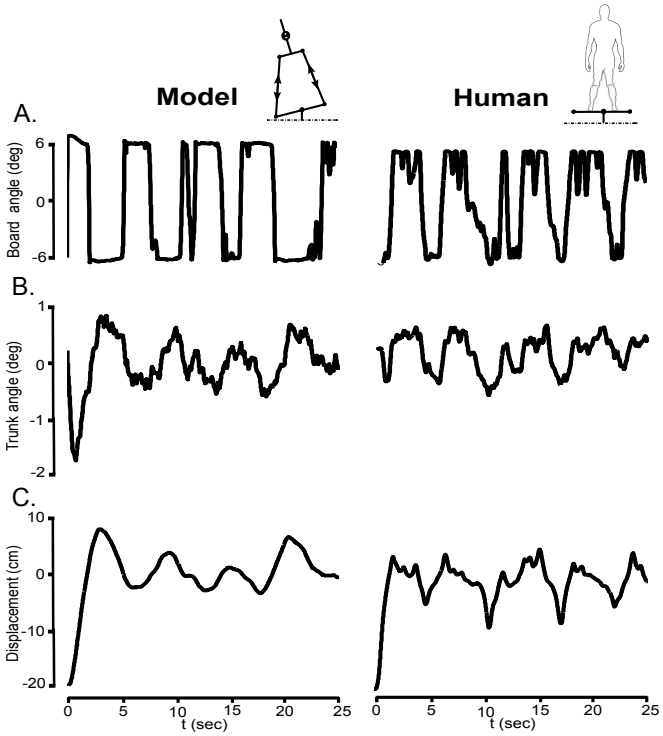

Fig. 6. Comparison of balancing motion of proposed control vs humans on a seesaw. (A) Board motion illustrates qualitatively similar intermittent rocking. (B) Trunk angle oscillates about zero degrees as both the model and the human subject try to maintain an upright trunk. (C) Displacement in COM's x position oscillates about zero. Human data is obtained from our motion capture experiments. The board and COM motions are comparable to human data in terms of amplitude and frequency (A,C).

from the first 25 seconds of a trial in our human expert experiment with simulation results. The qualitative similarity in board, trunk and COM motion supports the visual realism of the model's motion. Apart from visually looking at the motion, measuring human-likeness is hard. Here, we use amplitude and frequency features of motion trajectories for this comparison. The amplitudes of trunk sway (± 0.5 deg) and COM displacement in x (± 5 cm) for the simulation compares with those of the human expert. Analyzing the frequency of the rocking motion of the board with fast fourier transformation reveals a characteristic frequency of about 0.2 Hz for both the simulation and human data.

IV. Discussion and Future Work

Motivated by an interest in human-like controllers for humanoids to increase their social acceptance, we investigated balancing for artistic performances on challenging surfaces. In particular, we hypothesized that humans prefer an intuitive task-space control for lateral balancing, developed a virtual model controller for this task, and compared with simulations of a planar model, the resulting balancing behavior against human lateral balancing on flat ground and on a seesaw as an example of a challenging surface. Our results show that the proposed controller can be tuned to respond to balance disturbances on flat ground in a human-like way (Fig. 4), and that the controller mimics human behavior on a seesaw including the failure to stabilize the board (Fig. 6). Although not providing conclusive evidence, the results support the hypothesis that humans prefer intuitive control in lateral balancing and serve as further evidence for task space control in humans [13].

Our results also point towards more human-like controllers for humanoid robots. Previous control design for lateral balancing in humanoids focused on optimal control techniques [8], [6], [7], [9]. Indeed, applying standard linear quadratic regulator (LQR) techniques to the seesaw balancing model, we confirmed that controllers exist which can simultaneously stabilize the trunk pose and the board angle. This observation indicates that the state-of-art control approaches in robotics may go beyond what humans can do. In the seesaw example, we find that it may be even difficult for humans to use non-intuitive coordinate systems. A stabilizing LQR controller of seesaw balancing can still be found if the coriolis and centrifugal contributions are neglected in the linearized dynamics matrix when computing control gains. The only difference between the resulting LQR control and the quasistatic virtual model control then becomes the choice of coordinate system on which the controls act. While this coordinate system is intuitive in virtual model control (Eq. 1), the resulting LQR gain matrix is dense and combines several configuration space variables in a non-intuitive way. This difference is sufficient to generate a stabilizing controller or not, and humans do not seem to be able to identify the non-intuitive coordinate system. It may be important to take these limitations into account when designing human-like controllers for humanoid robots.

We plan to extend this work in three ways. First, we plan to use the proposed control strategy for other challenging balancing tasks such as bongo boarding. The successful interpretation of human balance on a bongo-board would further solidify the evidence for task space control in humans. As a final step towards confirming our hypotheses, we plan to interpret the proposed control with muscle reflexes and compare resultant EMG responses to humans as in [20]. While task space control may be preferred by humans, it remains open how they learn the actual controller including the specific task goals. We are interested in this fundamental question and plan to use the developed control framework to better understand motor learning in humans. Finally, we seek to transfer the proposed control to applications in graphics and entertainment robotics for the generation of human-like behavior during artistic performances on challenging surfaces.

ACKNOWLEDGEMENT

The authors would like to thank Justin Macey for helping with motion capture experiments.

References

[1] J. K. Hodgins and M. H. Raibert, "Biped gymnastics," *Int. J. Rob. Res.*, vol. 9, no. 2, pp. 115–132, Mar. 1990.

[2] Y. Zheng and K. Yamane, "Ball walker: A case study of humanoid robot locomotion in non-stationary environments," in *IEEE International Conference on Robotics and Automation*, 2011, pp. 2021–2028.

[3] S. Kajita, F. Kanehiro, K. Kaneko, K. Fujiwara, K. Harada, K. Yokoi, and H. Hirukawa, "Biped walking pattern generation by using preview control of zero-moment point," in *Proceedings of the IEEE International Conference on Robotics and Automation*, vol. 2, Sept 2003, pp. 1620–1626.

[4] B. Stephens, "Humanoid push recovery," in *7th IEEE-RAS International Conference on Humanoid Robots*, 2007, pp. 589–595.

[5] C. E. Bauby and A. D. Kuo, "Active control of lateral balance in human walking," *Journal of biomechanics*, vol. 33, no. 11, pp. 1433–1440, 2000.

[6] S. O. Anderson and J. K. Hodgins, "Adaptive torque-based control of a humanoid robot on an unstable platform," *10th IEEE-RAS International Conference on Humanoid Robots*, pp. 511–517, Dec. 2010.

[7] ——, "Informed priority control for humanoids," in *11th IEEE-RAS International Conference on Humanoid Robots*, 2011, pp. 416–422.

[8] S.-H. Hyon, "Compliant terrain adaptation for biped humanoids without measuring ground surface and contact forces." *IEEE Transactions on Robotics*, no. 1, pp. 171–178, 2010.

[9] U. Nagarajan and K. Yamane, "Universal balancing controller for robust lateral stabilization of bipedal robots in dynamic, unstable environments," *IEEE Intl Conf. on Robotics and Automation*, 2014.

[10] D. A. Winter, "Human balance and posture control during standing and walking," *Gait & posture*, vol. 3, no. 4, pp. 193–214, 1995.

[11] Z. Matjačić, M. Voigt, D. Popović, and T. Sinkjær, "Functional postural responses after perturbations in multiple directions in a standing man: a principle of decoupled control," *Journal of biomechanics*, vol. 34, no. 2, pp. 187–196, 2001.

[12] S. Rietdyk, A. Patla, D. Winter, M. Ishac, and C. Little, "Balance recovery from medio-lateral perturbations of the upper body during standing," *Journal of biomechanics*, vol. 32, no. 11, pp. 1149–1158, 1999.

[13] C. M. Harris and D. M. Wolpert, "Signal-dependent noise determines motor planning," *Nature*, vol. 394, no. 6695, pp. 780–784, 1998.

[14] E. Burdet, R. Osu, D. W. Franklin, T. E. Milner, and M. Kawato, "The central nervous system stabilizes unstable dynamics by learning optimal impedance," *Nature*, vol. 414, no. 6862, pp. 446–449, 2001.

[15] J. Pratt, "Virtual Model Control: An Intuitive Approach for Bipedal Locomotion," *The International Journal of Robotics Research*, vol. 20, no. 2, pp. 129–143, Feb. 2001.

[16] A. Hofmann, M. Popovic, and H. Herr, "Exploiting angular momentum to enhance bipedal center-of-mass control," in *IEEE International Conference on Robotics and Automation*, May 2009, pp. 4423–4429.

[17] J. G. Buckley, D. O'Driscoll, and S. J. Bennett, "Postural sway and active balance performance in highly active lower-limb amputees," *American journal of physical medicine & rehabilitation*, vol. 81, no. 1, pp. 13–20, 2002.

[18] D. A. Winter, *Biomechanics and motor control of human movement*, 4th ed. Hoboken, N.J.: Wiley, 2009.

[19] A. A. Faisal, L. P. Selen, and D. M. Wolpert, "Noise in the nervous system," *Nature Reviews Neuroscience*, vol. 9, no. 4, pp. 292–303, 2008.

[20] R. Desai and H. Geyer, "Muscle-reflex control of robust swing leg placement," in *IEEE International Conference on Robotics and Automation*, May 2013, pp. 2169–2174.